THE JOURNAL OF PHYSICAL CHEMISTRY Letters

Letter

pubs.acs.org/JPCL

Fluorescence from Multiple Chromophore Hydrogen-Bonding States in the Far-Red Protein TagRFP675

Patrick E. Konold,[†,‡] Eunjin Yoon,[§] Junghwa Lee,[§] Samantha L. Allen,[†,‡] Prem P. Chapagain,[∥] Bernard S. Gerstman,[∥] Chola K. Regmi,[∥,⊥] Kiryl D. Piatkevich,[#] Vladislav V. Verkhusha,[▽] Taiha Joo,*[,§] and Ralph Jimenez*[,†,‡]

[†]JILA, University of Colorado and NIST, Boulder, Colorado 80309, United States

[‡]Department of Chemistry & Biochemistry, University of Colorado, Boulder, Colorado 80309, United States

[§]Department of Chemistry, Pohang University of Science and Technology (POSTECH), Pohang, South Korea 790-784

[∥]Department of Physics, Florida International University, Miami, Florida 33199, United States

[⊥]Department of Physics, Virginia Tech, Blacksburg, Virginia 24061, United States

[#]Massachusetts Institute of Technology Media Lab, Massachusetts Institute of Technology, Cambridge, Massachusetts 02139, United States

[▽]Department of Anatomy & Structural Biology, Albert Einstein College of Medicine, Bronx, New York 10461, United States

Supporting Information

ABSTRACT: Far-red fluorescent proteins are critical for in vivo imaging applications, but the relative importance of structure versus dynamics in generating large Stokes-shifted emission is unclear. The unusually red-shifted emission of TagRFP675, a derivative of mKate, has been attributed to the multiple hydrogen bonds with the chromophore *N*-acylimine carbonyl. We characterized TagRFP675 and point mutants designed to perturb these hydrogen bonds with spectrally resolved transient grating and time-resolved fluorescence (TRF) spectroscopies supported by molecular dynamics simulations. TRF results for TagRFP675 and the mKate/M41Q variant show picosecond time scale red-shifts followed by nanosecond time blue-shifts. Global analysis of the TRF spectra reveals spectrally distinct emitting states that do not interconvert during the S_1 lifetime. These dynamics originate from photoexcitation of a mixed ground-state population of acylimine hydrogen bond conformers. Strategically tuning the chromophore environment in TagRFP675 might stabilize the most red-shifted conformation and result in a variant with a larger Stokes shift.

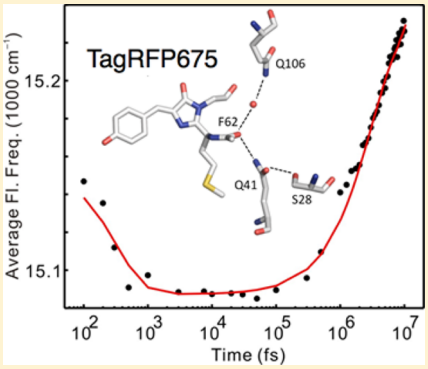

Red FPs (RFPs) with excitation and emission wavelengths beyond 650 nm (15380 cm^{-1}) are eagerly sought for in vivo imaging because they offer the prospect of lower autofluorescence background, lower light scattering, and higher tissue transmission relative to shorter-wavelength fluorophores.[1−4] Accordingly, molecular engineering of new RFPs with large Stokes-shifted emission is an important topic. Hydrogen-bonding to the *N*-acylimine carbonyl of the chromophore has been observed in the most red-emitting RFPs, including mNeptune, mCardinal, eqFP650, eqFP670, mRojoA, mRouge, and mPlum.[5−11] The reddest-emitting GFP-like protein with a reported crystal structure, TagRFP675,[9,12,13] contains an *N*-acylimine carbonyl with two hydrogen bonds, neither of which is present in its predecessor mKate (Figure 1). One arises from a direct interaction with the Q41 side chain, while the other involves a water molecule supported by tertiary interactions with the amide group of Q106.

Although hydrogen bonding to the *N*-acylimine carbonyl is strongly correlated with a large Stokes shift, the mechanism is still in question. We previously investigated mPlum, which has only a single hydrogen bond at this position.[14−16] Utilizing spectrally resolved transient grating (SRTG) spectroscopy and molecular dynamics (MD) simulations on a series of point mutants, we found that its red-shifted emission correlates with picosecond time scale switching between direct and water-mediated E16−I65 hydrogen-bonding interactions.[14] Faraji and Krylov explained this effect with quantum mechanics/molecular mechanics (QM/MM) calculations revealing the electron density increase at the carbonyl oxygen in S_1 and the relatively better electron accepting ability of a water-mediated hydrogen bond relative to a direct interaction with E16.[17] More recent femtosecond time-resolved fluorescence spectra (TRFS) revealed a 37 ps time scale for excited-state interconversion between the direct and water-mediated hydrogen-bonding

Received: May 28, 2016
Accepted: July 22, 2016

 © XXXX American Chemical Society

DOI: 10.1021/acs.jpclett.6b01172
J. Phys. Chem. Lett. 2016, 7, 3046−3051

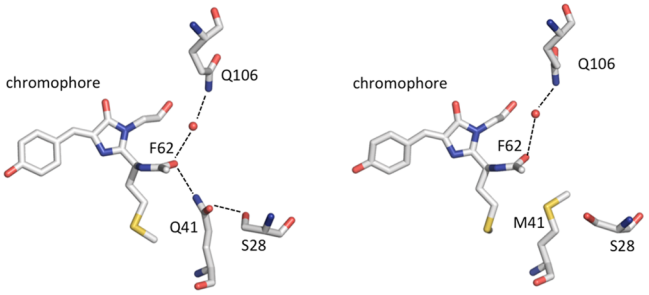

Figure 1. Chromophore *N*-acylimine region from the crystal structures of (left panel) TagRFP675 (PDB entry 4KGF) and (right panel) mKate (PDB entry 3BXB). Hydrogen bonds are represented as dashed black lines; atoms are colored by atom type; water molecules are shown as red spheres.

structures.[18] We now report the excited-state dynamics of TagRFP675 investigated with SRTG and TRFS measurements and MD simulations. The fluorescence dynamics are explained in terms of heterogeneous emission resulting from distinct acylimine hydrogen-bonding structures.

One set of TagRFP675 mutants was designed to perturb the water-mediated hydrogen bond between Q106 and F62. The Q106M mutation disrupts the interaction by replacing one of the participating side chains with a group of similar size without a hydrogen-bond donor, whereas the F62A mutation alters the sterics, as was previously demonstrated for mPlum.[14] To probe the Q41 interaction, we added this hydrogen-bonding group to the parent mKate (i.e., mKate/M41Q), and removed it from TagRFP675 (i.e., TagRFP675/Q41M). Absorption peaks of these variants (Table 1) fall between 16 670 and 17 090 cm^{-1}

Table 1. Steady-State Absorption and Emission Data for mKate and TagRFP675 Variants

mutant	absorption peak (cm^{-1})	emission peak (cm^{-1})	Stokes shift (cm^{-1})
mKate	17 010	15 750	1260
mKate/M41Q	17 270	15 310	1960
TagRFP675	16 670	14 810	1860
TagRFP675/F62A	16 720	15 200	1520
TagRFP675/Q106M	16 950	15 430	1520
Tag RFP675/F62A/Q106M	17 010	15 580	1430
TagRFP675/Q41M	16 950	15 550	1400

(585−600 nm). As expected, disruption of the water-mediated hydrogen bond network by single- or double-point mutations leads to blue-shifted emission in the TagFP675/F62A, Q106M, and F62A/Q106M variants. Addition of a hydrogen bond at the *N*-acylimine carbonyl in mKate/M41Q leads to a 700 cm^{-1} increase in Stokes shift, while its removal in TagRFP675/Q41M yields a 460 cm^{-1} decrease.

SRTG measurements were employed to characterize ground- and excited-state dynamics of the RFPs. The transient spectral features shown in the contour plots of Figure 2a,b for TagRFP675 and mKate/M41Q correspond to the ground-state bleach (GSB) and stimulated emission (SE) responses. SRTG spectra of the other RFPs (Figure S2) show a similar bimodal shape, except for TagRFP675/Q41M and mKate, where the SE contribution is present only as a shoulder on the GSB peak. The SE contribution was fitted to a Gaussian function, and the peak frequency versus time shows a red-shift

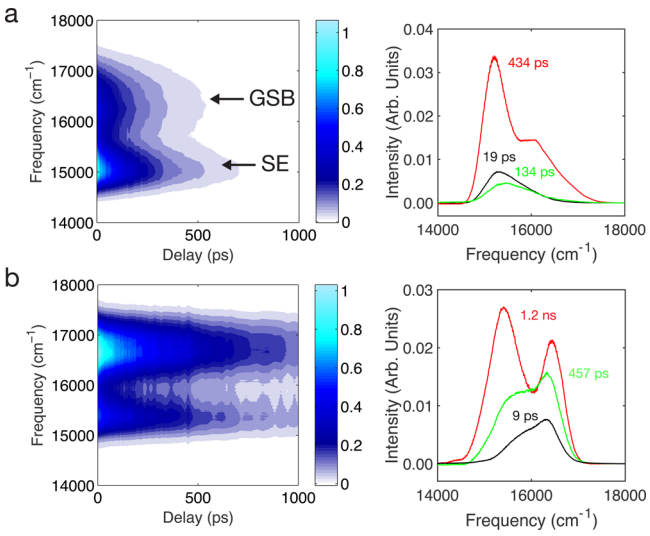

Figure 2. SRTG spectra and DAS for (a) TagRFP675 and (b) mKate/M41Q.

with biexponential kinetics with, for example, 17 and 397 ps components for TagRFP675, and a total spectral shift of 77 cm^{-1}. Parameters for the other RFPs are given in Table S1. Note that SRTG differs from transient absorption in that the third-order optical response is detected in quadrature, and as a consequence, SRTG signals are positive and time evolution of the intensity is twice as fast.[19] Time constants reported in Figure 2 and Tables S1 and S2 are corrected accordingly. This transient red-shift is consistent with excited-state solvation dynamics, although the magnitude of the observed shift is much smaller than the total Stokes shift because of the limited excitation bandwidth and the presence of an overlapping ESA band, as discussed previously for mPlum.[14] Global analysis revealed the SRTG measurements are well fit by three components with time scales ranging from a few picoseconds to almost 2 ns (Figures 2 and S3 and Table S2). The amplitudes of all decay associated spectra (DAS) components extend over both the GSB and SE bands, indicating that the transitions are largely overlapped. In all cases, amplitudes of the DAS are positive at all wavelengths, indicating that only decay components and no risetimes are observed. The SE peak shifts are therefore not due to a spectral red-shift as expected from conventional solvation dynamics but instead are caused by the lifetime decays of multiple spectral forms.

To further evaluate the dynamics of TagRFP675 and mKate/M41Q, we employed TRFS. Time-resolved area-normalized spectra (TRANES) of these RFPs are shown in Figure 3. These data sets comprise spectra from fluorescence upconversion for time delays <1 ns stitched together with spectra from time-correlated single-photon counting for longer times (methods are described in the Supporting Information). Although TRFS often reveal transient red-shifts associated with solvation dynamics, these RFPs show atypical behavior. The total spectral shifts are only a small proportion of their total Stokes shifts, and, most unusually, the time-evolution of the first moments show initial red-shifts followed by nanosecond time scale blue-shifts (Figure S5 and fit parameters collected in Table S3). Although neither RFP shows an isoemissive point at all times, both show an isoemissive point for part of the experimental time window. This spectral behavior is a hallmark of a system with a small number of discrete emitting states.[20]

DOI: 10.1021/acs.jpclett.6b01172
J. Phys. Chem. Lett. 2016, 7, 3046−3051

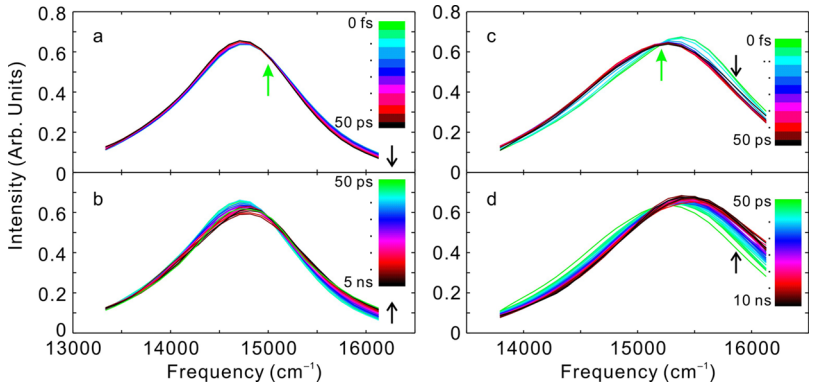

Figure 3. TRANES spectra constructed from femtosecond and picosecond TRFS (a) TagRFP675 from 0 to 50 ps and (b) TagRFP675 from 50 ps to 5 ns (c) mKate/M41Q from 0 to 50 ps and (d) mKate/M41Q from 50 ps to 10 ns. Actual times for each curve can be obtained from the dots in Figure S5. Time increases in the direction of the black arrows. The green arrows indicate isoemissive points.

For TagRFP675, TRANES show an isoemissive point near 15 000 cm^{-1} at times less than ~100 ps (Figure 3a), whereas mKate/M41Q (Figure 3c) shows isoemissive behavior at very short times, <1 ps.

The DAS of TagRFP675 from global analysis fitting of the TRFS (Figure 4a) consists of four components, whereas

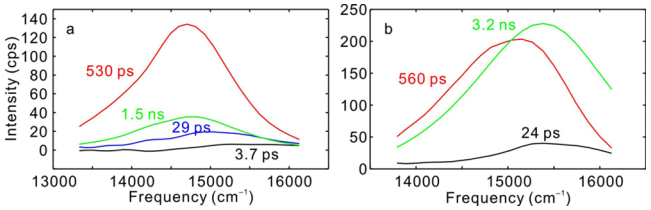

Figure 4. DAS from global analysis of TRFS for (a) TagRFP675 and (b) mKate/M41Q.

mKate/M41Q (Figure 4b) shows three components. For both RFPs, the components are decays at all wavelengths, which means that no population redistribution occurs, and the mixture of spectral forms in S_1 therefore results from the excitation of a mixed S_0 population. In both cases, there is a segregation of time scales between the fastest dynamics and the two longest components, which are of the largest amplitudes. Also, in both FPs, the longest lifetime is not associated with the most red-shifted state, which explains the origin of the nanosecond time scale blue shifts. The presence of the isoemissive points in both FPs is a result of a segregation in time scales. For mKate/M41Q, the 24 ps component is much faster than the 560 ps and 3.2 ns components which constitute the majority of the emission decay. At early times, this system appears to be nearly two-state and therefore shows an isoemissive point. Similar behavior is observed in TagRFP675.

Because the DAS of TagRFP675 and mKate/M41Q imply that multiple spectral forms originate in the ground state, we performed 50 ns classical MD simulations (described in the Supporting Information) to determine if they show a small number of acylimine hydrogen-bond structures that could explain these spectral states. Figure 5a,b displays the time

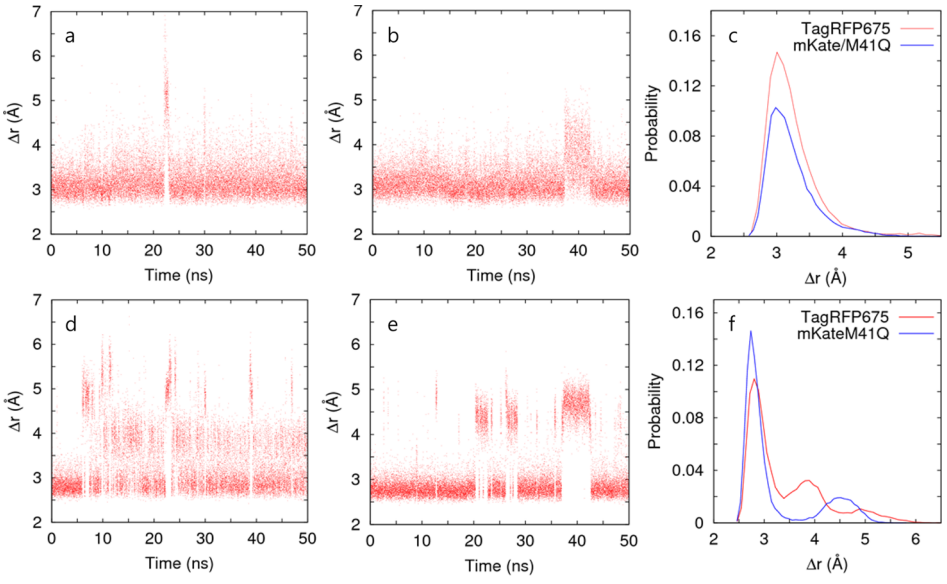

Figure 5. Fluctuations in separation (Δr) between the nitrogen atom in the side chain of Q41 and the *N*-acylimine oxygen of F62 for (a) TagRFP675 and (b) mKate/M41Q. In panel c, these results are given as histograms. Fluctuations of the distance (Δr) between oxygen atoms in the side chains of S28 and Q41 for (d) TagRFP675 and (e) mKate/M41Q. In panel f, these results are given as histograms, with data sorted into 50 bins over the plotted range.

DOI: 10.1021/acs.jpclett.6b01172
J. Phys. Chem. Lett. 2016, 7, 3046−3051

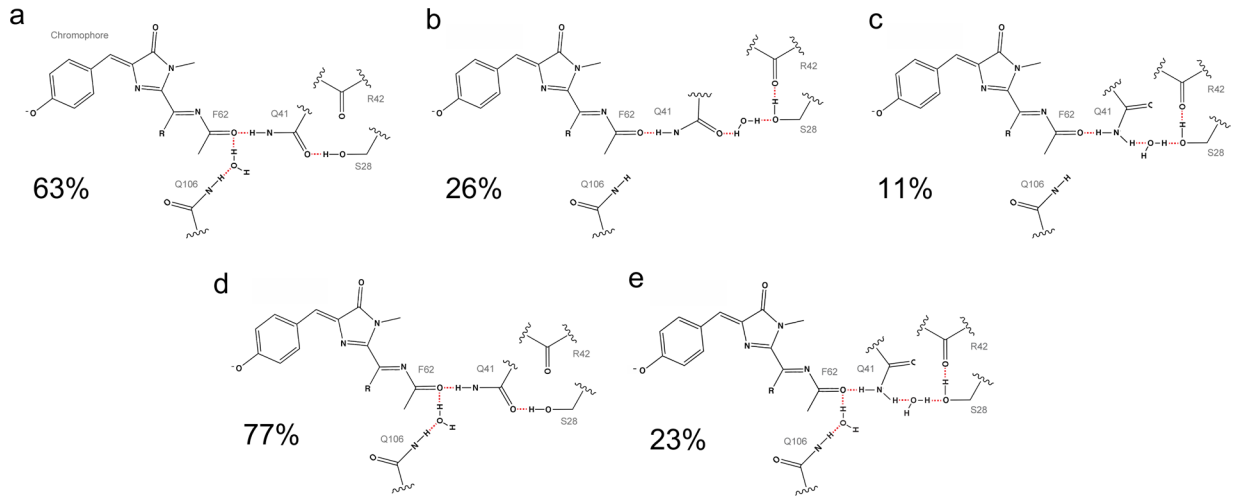

Figure 6. Configurations of hydrogen bond network in acylimine region from MD for TagRFP675 (a–c) and for mKate/M41Q (d, e). Percentages were calculated based on the O–O distance between S28 and Q41. The three states in TagRFP675 correspond to $\Delta r < 3.5$ Å, 3.5 Å $\leq \Delta r < 4.5$ Å, and $\Delta r \geq 4.5$ Å. In mKate/M41Q, the two states correspond to $\Delta r < 3.5$ Å and $\Delta r \geq 3.5$ Å.

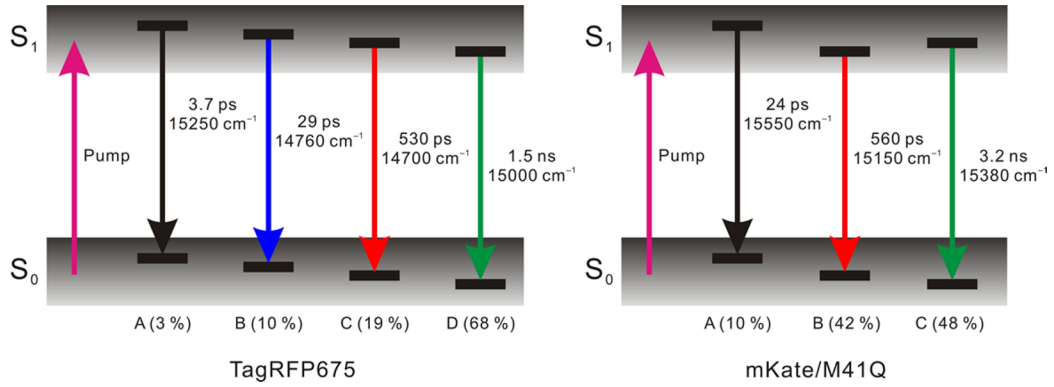

Figure 7. Level diagrams describing photophysics of TagRFP675 and mKate/M41Q. Initial photoexcitation from a distribution of conformers in S_0 creates excited-state populations with a distribution of conformers. Relative populations are noted.

trajectories of the distance (Δr) between the nitrogen atom in the Q41 side chain and the *N*-acylimine carbonyl oxygen of F62 for both RFPs. Both variants largely maintain a conformation with a direct hydrogen bond (~3.5 Å), with rare excursions into a water-mediated structure (~4.5 Å) or non-hydrogen-bonded state (≳5 Å). The interaction between F62 and Q106, which is the other immediate interaction, showed contrasting behavior for the two FPs. In TagRFP675, the water molecule is mobile and moves into a water-mediated hydrogen bond with Q41. However, in mKate/M41Q, the Q106–F62 hydrogen bond is more stable, and this water molecule never leaves. Neither RFP shows a direct F62–Q106 hydrogen bond during the 50 ns trajectories.

The S28–Q41 hydrogen bond plays an important role in orienting the Q41 side chain for its interaction with F62. In TagRFP675 (Figure 5d,f), this interaction converts between three states, whereas mKate/M41Q converts between two states (Figure 5e,f). For the dominant configuration in TagRFP675 (Figure 6a), S28 hydrogen bonds with Q41. In another orientation, it hydrogen bonds to R42, resulting in two structures. In one, the Q41 amino group interacts with S28 via a water-mediated hydrogen bond (Figure 6b) while the other is a water-mediated hydrogen bond with the carbonyl (Figure 6c). Both structures result in an extended network: F62–Q41–water–S28–R42 involving a water molecule that more frequently hydrogen-bonds between F62 and Q106. The S28 and Q41 side chain dynamics, along with this mobile water molecule, lead to a highly dynamic network in TagRFP675. Only two structures are observed for mKate/M41Q. In both, a water molecule is found between F62 and Q106. The dominant structure contains a direct S28–Q41 carbonyl interaction (Figure 6d), whereas another contains S28 interacting directly with both Q41 and R42 (Figure 6e). Figure 6 shows the percentage of time spent in each of these conformations during the 50 ns trajectory.

The SRTG and TRF results on TagRFP675 and mKate/M41Q both reveal multiple picosecond/nanosecond components, and more significantly, neither measurement reveals risetimes. The excitation and detection conditions of the two experiments differ and consequently prepare and probe different mixtures of spectral forms. SRTG measurement was performed with large bandwidth pulse spectra in which excitation and detection spans the red-edge of the absorption and part of the emission spectra (Figure S1). The excitation spectrum therefore creates a hole in the absorption spectrum. Because the system is inhomogeneously broadened because of the multiple ground-state spectral components, the SE band does not significantly red shift, and the GSB component does not significantly blue-shift. In contrast, TRF was performed with narrow-band excitation spectra near the peak absorption

DOI: 10.1021/acs.jpclett.6b01172
J. Phys. Chem. Lett. 2016, 7, 3046–3051

wavelength and wide-band, spectrally resolved detection. Nevertheless, results from both measurements consistently point to the parallel decay of an optically excited set of states. Additional support for the presence of multiple ground states is provided by steady-state fluorescence measurements on both FPs (Figure S6) showing that the emission peak wavelength varies as excitation wavelength is tuned across the absorption band.[9]

Our model of the fluorescence dynamics is based on the TRFS global analysis results, which permits a complete view of the emitting states. For a mixture of noninterconverting emitting states with distinct lifetimes, the spectrum of each component can be obtained from the DAS. Because the analysis reveals well-separated decay time constants, we expect that the DAS components correspond to distinct spectral states. The peak energy and relative weight of each component is taken from the DAS, assuming equal excitation probabilities. The resulting diagrams (Figure 7a,b) depict the photoexcitation of a mixture of ground states, creating a set of four emitting states in the case of TagRFP675 and three states for mKate/M41Q. The >500 ps components represent the predominant emitting states of each FP and are consistent with the measured fluorescence lifetimes.[9,12,13]

Next, we consider possible structural origins of these spectral forms. The SRTG and steady-state spectra show that perturbation of the water-mediated hydrogen bond between Q106 and the acylimine in the TagRFP675/F62A, Q106M, and F62A/Q106M mutants leads to a moderate decrease (~300 cm^{-1}) in Stokes shift and a minor effect on the excited-state time scales. These differences may be attributed to a change in flexibility of the acylimine carbonyl given a reduction in steric hindrance of the side chain in the F62A mutation and loss of the water-mediated hydrogen bond in the Q106M mutation. The SRTG data also reveal that variants lacking a direct hydrogen bond to the Q41 side chain (mKate, TagRFP675/Q41M) do not show picosecond/nanosecond dynamics. In contrast, the presence of a hydrogen-bond donor to the acylimine in mKate/M41Q leads to a dramatically larger Stokes shift on par with TagRFP675 and similar excited-state time scales. It seems likely that the Q41−S28 interaction both indirectly modulates the hydrogen bond strength of Q41−F62 and modulates the flexibility of an extended network that interconverts between states. These results indicate that the direct hydrogen bond with the Q41 side chain along with an extended hydrogen bond network has the largest impact on the Stokes shift of TagRFP675. We therefore suggest that the spectral forms identified in the DAS originate from distinct structures of the F62−Q41−S28 hydrogen-bonding network, such as those illustrated in Figure 6. It is tempting to make specific assignments of these spectral forms to structures by relying on the amplitudes of the DAS spectra from TRF and the populations from the ground-state MD simulation. However, these assignments are likely to be inaccurate because at least the photoexcitation probability for each spectral form under the excitation wavelength and bandwidth needs to be taken into account. To produce reliable assignments, temperature and excitation wavelength-dependent TRF measurements are necessary and will be the subject of future research.

It is remarkable that small changes in hydrogen-bonding result in a 100-fold variation in excited-state lifetime. Understanding this effect will be critical for designing RFPs with high fluorescence yields, especially in light of the low brightness of most RFPs with large Stokes shifts.[21] Although our results emphasize the importance of the acylimine region for the Stokes shift, hydrogen bonding to the chromophore p-hydroxyphenyl group also impacts the fluorescence properties. We also examined these interactions in our MD simulations of TagRFP675, mKate/M41Q, and mKate and find they are very similar. In all three FPs, the phenolate interacts predominantly with E141 via two water-mediated hydrogen bonds, though interaction with N143 to a minor extent is also observed. Three movies showing hydrogen bonds in the phenolate and acylimine regions are provided in the Supporting Information. Because the dynamics are very similar for three RFPs with widely varying Stokes shift, it appears that interactions of the phenolate do not play a major role in the Stokes shift, but instead their role is to stabilize the fluorescent cis-conformation of the chromophore. A previous study of TagRFP675 revealed pH-dependent changes involving protonation of the p-hydroxyphenyl group and rearrangements of the N143, N158, and R197 side chains. Furthermore, the fluorescence blue-shifts and the intensity decreases several fold when the pH is decreased, with a midpoint near pH 5.5.[9] For the pH 8.0 buffer employed in the current study (which differs from that used in ref 9), the TagRFP675 sample will contain a small percentage of the nonfluorescent structure. We propose that this alternate hydroxyphenyl structure corresponds to the 3.7 ps, blue-shifted state in Figure 7.

The dynamics of TagRFP675 are strikingly different from those of mPlum, which shows simple two-state emission behavior.[18] QM/MM calculations on mPlum show that the partial charge of the acylimine oxygen increases upon electronic excitation and that the S_1 energy of the water-mediated hydrogen bonded state is below that of the direct hydrogen-bonded state.[17] When the mixed population of direct and water-mediated conformers in S_0 is photoexcited, the direct subpopulation relaxes (on a 37 ps time scale) to a water-mediated state with lower energy, whereas the water-mediated population only slightly reorganizes. In contrast, the presence of two acylimine-side chain interactions in TagRFP675 leads to several different hydrogen bond conformations in S_0, which unlike in mPlum, do not convert to a dominant configuration in S_1. Another point of contrast is that the most frequent reconfiguration of the hydrogen bond network observed in MD does not involve immediate hydrogen bonding to the acylimine but rather the secondary set of interactions with the Q41 side chain. These hydrogen bond rearrangements could impact the electronic energies by influencing the orientation of the Q41 hydrogen-bond donating groups to the acylimine carbonyl, in turn modulating the electron-accepting capability of the donor groups.

In conclusion, our central finding is that the presence of two acylimine hydrogen-bonding interactions in TagRFP675 and mKate/M41Q leads to a heterogeneous system with multiple emitting forms that do not interconvert on the time scale of the S_1 lifetime. The absence of a continuous solvation process with amplitude of red-shift comparable to the total Stokes shift of TagRFP675 implies that the environment is fairly rigid and only permits energetically significant relaxation along degrees of freedom involving the hydrogen bonds near the acylimine. We suggest that the majority of the Stokes shift in TagRFP675 and mKate/M41Q occurs via subpicosecond chromophore relaxation which is not observed in the current measurements because of insufficient time resolution, though such dynamics were proposed to be the origin of a 160 fs time scale observed in mPlum.[18] Another important finding is that the most red-

DOI: 10.1021/acs.jpclett.6b01172
J. Phys. Chem. Lett. 2016, 7, 3046−3051

shifted component (530 ps lifetime) in the DAS of TagRFP675 peaks at 680 nm. Strategically tuning the chromophore environment to stabilize the conformation corresponding to this spectral form would yield an improved longer-wavelength emitting RFP for in vivo imaging.

■ ASSOCIATED CONTENT

Supporting Information

The Supporting Information is available free of charge on the ACS Publications website at DOI: 10.1021/acs.jpclett.6b01172.

Experimental and computational methods, additional data, and analysis results for SRTG and TRF (PDF)

Movie of hydrogen bonds in the phenolate and acylimine for mKate (MPG)

Movie of hydrogen bonds in the phenolate and acylimine for mKate/M41Q (MPG)

Movie of hydrogen bonds in the phenolate and acylimine for TagRFP675 (MPG)

■ AUTHOR INFORMATION

Corresponding Authors

*E-mail: rjimenez@jila.colorado.edu.

*E-mail: thjoo@postech.ac.kr.

Notes

The authors declare no competing financial interest.

■ ACKNOWLEDGMENTS

This work was supported by the NSF Physics Frontier Center at JILA and the National Institutes of Health (GM105997 and GM108579 to V.V.V and SC3GM096903 to P.P.C.). S.L.A. was supported by the University of Colorado Molecular Biophysics Training Grant (T32 GM065103). T.J. acknowledges the financial support by the Global Research Laboratory Program (2009-00439) through the National Research Foundation of Korea. R.J. is a staff member in the Quantum Physics Division of the National Institute of Standards and Technology (NIST). Certain commercial equipment, instruments, or materials are identified in this paper in order to specify the experimental procedure adequately. Such identification is not intended to imply recommendation or endorsement by the NIST, nor is it intended to imply that the materials or equipment identified are necessarily the best available for the purpose.

■ REFERENCES

(1) Wu, B.; Piatkevich, K. D.; Lionnet, T.; Singer, R. H.; Verkhusha, V. V. Modern Fluorescent Proteins and Imaging Technologies to Study Gene Expression, Nuclear Localization, and Dynamics. *Curr. Opin. Cell Biol.* **2011**, *23*, 310−317.

(2) Shcherbakova, D. M.; Subach, O. M.; Verkhusha, V. V. Red Fluorescent Proteins: Advanced Imaging Applications and Future Design. *Angew. Chem., Int. Ed.* **2012**, *51*, 10724−10738.

(3) Chudakov, D. M.; Matz, M. V.; Lukyanov, S.; Lukyanov, K. A. Fluorescent Proteins and Their Applications in Imaging Living Cells and Tissues. *Physiol. Rev.* **2010**, *90*, 1103−1163.

(4) Subach, F. V.; Piatkevich, K. D.; Verkhusha, V. V. Directed Molecular Evolution to Design Advanced Red Fluorescent Proteins. *Nat. Methods* **2011**, *8*, 1019−1026.

(5) Lin, M. Z.; McKeown, M. R.; Ng, H.-L.; Aguilera, T. A.; Shaner, N. C.; Campbell, R. E.; Adams, S. R.; Gross, L. A.; Ma, W.; Alber, T.; Tsien, R. Y. Autofluorescent Proteins with Excitation in the Optical Window for Intravital Imaging in Mammals. *Chem. Biol.* **2009**, *16*, 1169−1179.

(6) Chu, J.; Haynes, R. D.; Corbel, S. Y.; Li, P.; Gonzalez-Gonzalez, E.; Burg, J. S.; Ataie, N. J.; Lam, A. J.; Cranfill, P. J.; Baird, M. A.; Davidson, M. W.; Ng, H.-L.; Garcia, K. C.; Contag, C. H.; Shen, K.; Blau, H. M.; Lin, M. Z. Non-Invasive Intravital Imaging of Cellular Differentiation with a Bright Red-Excitable Fluorescent Protein. *Nat. Methods* **2014**, *11*, 572−578.

(7) Pletnev, S.; Pletneva, N. V.; Souslova, E. A.; Chudakov, D. M.; Lukyanov, S.; Wlodawer, A.; Dauter, Z.; Pletnev, V. Structural Basis for Bathochromic Shift of Fluorescence in Far-Red Fluorescent Proteins eqFP650 and eqFP670. *Acta Crystallogr., Sect. D: Biol. Crystallogr.* **2012**, *68*, 1088−1097.

(8) Chica, R. A.; Moore, M. M.; Allen, B. D.; Mayo, S. L. Generation of Longer Emission Wavelength Red Fluorescent Proteins Using Computationally Designed Libraries. *Proc. Natl. Acad. Sci. U. S. A.* **2010**, *107*, 20257−20262.

(9) Piatkevich, K. D.; Malashkevich, V. N.; Morozova, K. S.; Nemkovich, N. A.; Almo, S. C.; Verkhusha, V. V. Extended Stokes Shift in Fluorescent Proteins: Chromophore-Protein Interactions in a near-Infrared TagRFP675 Variant. *Sci. Rep.* **2013**, *3*, 1847.

(10) Wang, L.; Jackson, W. C.; Steinbach, P. A.; Tsien, R. Y. Evolution of New Nonantibody Proteins Via Iterative Somatic Hypermutation. *Proc. Natl. Acad. Sci. U. S. A.* **2004**, *101*, 16745−16749.

(11) Li, Z.; Zhang, Z.; Bi, L.; Cui, Z.; Deng, J.; Wang, D.; Zhang, X.-E. Mutagenesis of mNeptune Red-Shifts Emission Spectrum to 681−685 nm. *PLoS One* **2016**, *11*, e0148749.

(12) Shcherbo, D.; Merzlyak, E. M.; Chepurnykh, T. V.; Fradkov, A. F.; Ermakova, G. V.; Solovieva, E. A.; Lukyanov, K. A.; Bogdanova, E. A.; Zaraisky, A. G.; Lukyanov, S.; Chudakov, D. M. Bright Far-Red Fluorescent Protein for Whole-Body Imaging. *Nat. Methods* **2007**, *4*, 741−746.

(13) Morozova, K. S.; Piatkevich, K. D.; Gould, T. J.; Zhang, J.; Bewersdorf, J.; Verkhusha, V. V. Far-Red Fluorescent Protein Excitable with Red Lasers for Flow Cytometry and Superresolution Sted Nanoscopy. *Biophys. J.* **2010**, *99*, L13−L15.

(14) Konold, P.; Regmi, C. K.; Chapagain, P. P.; Gerstman, B. S.; Jimenez, R. Hydrogen Bond Flexibility Correlates with Stokes Shift in mPlum Variants. *J. Phys. Chem. B* **2014**, *118*, 2940−8.

(15) Abbyad, P.; Childs, W.; Shi, X.; Boxer, S. G. Dynamic Stokes Shift in Green Fluorescent Protein Variants. *Proc. Natl. Acad. Sci. U. S. A.* **2007**, *104*, 20189−20194.

(16) Shu, X.; Wang, L.; Colip, L.; Kallio, K.; Remington, S. J. Unique Interactions between the Chromophore and Glutamate 16 Lead to Far-Red Emission in a Red Fluorescent Protein. *Protein Sci.* **2009**, *18*, 460−466.

(17) Faraji, S.; Krylov, A. I. On the Nature of an Extended Stokes Shift in the mPlum Fluorescent Protein. *J. Phys. Chem. B* **2015**, *119*, 13052−13062.

(18) Yoon, K.; Konold, P. E.; Lee, J.; Joo, T.; Jimenez, R. Far-Red Emission of mPlum Fluorescent Protein Results from Excited-State Interconversion between Chromophore Hydrogen-Bonding States. *J. Phys. Chem. Lett.* **2016**, *7*, 2170.

(19) Joo, T.; Jia, Y.; Yu, J. Y.; Lang, M. J.; Fleming, G. R. Third-Order Nonlinear Time Domain Probes of Solvation Dynamics. *J. Chem. Phys.* **1996**, *104*, 6089−6108.

(20) Periasamy, N. Heterogeneity of Fluorescence Determined by the Method of Area-Normalized Time-Resolved Emission Spectroscopy. *Methods Enzymol.* **2008**, *450*, 21−35.

(21) Cranfill, P. J.; Sell, B. R.; Baird, M. A.; Allen, J. R.; Lavagnino, Z.; de Gruiter, H. M.; Kremers, G.-J.; Davidson, M. W.; Ustione, A.; Piston, D. W. Quantitative Assessment of Fluorescent Proteins. *Nat. Methods* **2016**, *13*, 557−562.

DOI: 10.1021/acs.jpclett.6b01172
J. Phys. Chem. Lett. 2016, 7, 3046−3051

Supporting Information for Fluorescence from Multiple Chromophore Hydrogen-Bonding States in the Far-Red Protein TagRFP675

Patrick E. Konold[1,2], Eunjin Yoon[3], Junghwa Lee[3], Samantha Allen,[1,2] Prem P. Chapagain[4], Bernard S. Gerstman[4], Chola K. Regmi[4,5], Kiryl D. Piatkevich[6], Vladislav V. Verkhusha,[7] Taiha Joo[3] and Ralph Jimenez[1,2,*]

[1] JILA, University of Colorado and NIST, Boulder, CO 80309

[2] Department of Chemistry & Biochemistry, University of Colorado, Boulder, CO 80309

[3] Department of Chemistry, Pohang University of Science and Technology (POSTECH), Pohang, South Korea 790-784

[4] Department of Physics, Florida International University, Miami, FL 33199

[5] Department of Physics, Virginia Tech, Blacksburg, VA 24061

[6] Massachusetts Institute of Technology Media Lab, Massachusetts Institute of Technology, Cambridge, MA 02139

[7] Department of Anatomy & Structural Biology, Albert Einstein College of Medicine, Bronx, NY 10461

[*] Correspondence should be addressed to R.J. (rjimenez@jila.colorado.edu) or T.J. (thoo@postech.ac.kr)

Contents:

Methods

SRTG Spectroscopy

Transient grating measurements were performed as previously described with the JILA MONSTR nonlinear optical platform.[1-2] Upon irradiation with 3 excitation pulses (20 fs, ~10 nJ/beam, 50 μm spot size, 20 kHz repetition rate), the spatially isolated four-wave mixing signal is emitted in the prescribed $\mathbf{k_s}=-\mathbf{k_1}+\mathbf{k_2}+\mathbf{k_3}$ phase matching direction. The excitation wavelength was chosen to maximize contrast between Ground State Bleach (GSB) and Stimulated Emission (SE) components, which varied slightly for each mutant. Measured excitation spectra are provided in Figure S1. The sample was refreshed with a spinning cell to mitigate photobleaching and accumulation of laser-induced photoproducts. The sample concentration (~50 μM; 0.15 peak optical density) and optical path length (0.5 mm) were selected to avoid protein aggregation and reabsorption of the nonlinear signal. The spectrally-resolved homodyne signal was collected as a function of the *T* time delay ($\mathbf{k_1}$ and $\mathbf{k_2}$ temporally overlapped) from a range of 0 to 1.3 ns, spaced logarithmically, with a background spectrum collected at -500 fs delay to eliminate contributions from excitation scatter and spontaneous emission. The baseline-subtracted spectra were fit to a sum of two Gaussians using a nonlinear least squares fitting algorithm. The SE peak center position and amplitude was extracted at each time delay and fit to multiexponential decays.

Femtosecond TRF

Output from a home-built cavity dumped optical parametric oscillator (OPO) employing a magnesium-doped periodically poled lithium niobate (MgO:PPLN) crystal as the gain medium was frequency-doubled in a 2 mm-thick lithium triborate (LBO) crystal to generate the pump pulse.[3] The pulse spectrum was 310 cm^{-1} FWHM and centered at 16670 cm^{-1} (600 nm) for the TRF of TagRFP675 and at 17540 cm^{-1} (570 nm) for mKate/M41Q. The excitation wavelength was tuned near the absorption maximum to wavelengths where the laser system gave nearly identical bandwidth excitation pulses (310 cm^{-1} FWHM) for the two measurements. The excitation wavelength for mKate/M41Q would 270 cm^{-1} blue-shifted from the absorption peak. For a room-temperature measurement, this difference in excitation conditions is unlikely to result in measurable differences on ps/ns timescales. The remaining infrared pulse energy was used for the gate pulse. Femtosecond time

resolution was achieved by sum frequency generation (SFG) between the fluorescence and the gate pulse in 300 μm-thick β-barium borate (BBO) crystal. The SFG signal was spectrally filtered by a double monochromator (DH10, Horiba Jobin Yvon) and detected by a photomultiplier (H6180-01, Hamamatsu) and a photon counter (SR400, Stanford Research). TRF spectra (TRFS) were measured directly without the spectral reconstruction by simultaneously controlling the phase matching angle of the BBO crystal, the time delay of the gate pulse, and the detected SFG wavelength. The instrument response function of the TRF setup was <200 fs (FWHM). A 200 μm-thick flow cell (Starna Inc.) containing the protein samples (~200 μM) was shaken to avoid any photodamage during the measurements. To avoid the scattering of the pump pulse and the second harmonic of the gate pulse, the blue edge of the fluorescence spectra was eliminated.

Picosecond TRF and TRF Anisotropy

The OPO used for the femtosecond TRF experiments was employed for Time-Correlated Single Photon Counting (TCSPC) to record picosecond-nanosecond TRFS. Details of the TCSPC setup have been presented elsewhere[4]. The fluorescence signal was collected and dispersed by a monochromator (SP-300i, Acton Research) and detected with an avalanche photodiode (ID-100-50-STD, ID Quantique). The instrument response function of the TCSPC system was 50 ps (FWHM). TCSPC time traces were obtained at every 5 nm step size to reconstruct the picosecond TRFS. Magic angle (54.7^{o}) detection was used to avoid the effect of polarization on timescales of the picosecond TRF measurement.

MD Simulations

Time series trajectories were obtained with explicit solvent, all-atom simulations using the NAMD molecular dynamics package with the CHARMM27 force field[5-6]. The initial X-ray crystallographic structures were obtained from the Protein Data Bank (TagRFP675 PDB 4KGF and mKate PDB 3BXB). We used CHARMM to make the amino acid substitutions in the TagRFP675 mutants F62A, Q106M, and F62A/Q106M as well as for the mKate/M41Q mutant. Force field parameters for the mature chromophore were adopted from the anionic GFP chromophore developed by Reuter *et al*. and from CHARMM27 parameters for

acylimine nitrogen[7]. The anionic form of the chromophore in the ground state was used. The VMD package was used to setup the system for simulations[8]. The initial structure of TagRFP675 with crystallographic water molecules was solvated using VMD. For all mutants, the box cutoff was set to 10 Å. For TagRFP675, this resulted in a simulation box of dimensions of 66 x 72 x 77 $Å^3$, with similar dimensions for the other mutants. Each solvated system for TagRFP675 and its variants was electrically neutralized by adding 1 Na^+ ion randomly in the bulk water. The final system contained about 35,000 atoms. The particle mesh Ewald method was used to treat long-range interactions with a 12 Å nonbonded cutoff[9]. Energy minimization was performed using the conjugate gradient and line search algorithm. The system was then heated for 90 ps with a linear gradient of 20K/6ps from 20 to 300 K. At 300 K, the system was equilibrated for 910 ps with a 2 fs integration time step in the NVT (constant number, volume, and temperature) ensemble. Langevin dynamics was used to maintain the temperature at 300 K. The production run was 50 ns using NVT dynamics with 2 fs time steps.

Protein Mutagenesis, Expression, and Purification

FPs were expressed with the pBAD vector containing the corresponding genes under control of the arabinose promoter. Point mutations were introduced with QuikChange mutagenesis using custom designed primers (IDT). Expression procedures differed slightly for the two primary lineages studied. For mKate and mutants, plasmids were transformed into Top10 *E. coli*, grown to OD_{600}=0.6 at 37 °C, followed by induction with 0.02% arabinose for 24 hours at 30 °C. Plasmids of TagRFP675 and mutants were transformed into the LMG194 *E. coli* strain, grown to OD_{600}=0.6 at 37 °C, followed by induction with 0.02% arabinose for 48 hours at 18 °C. Samples were purified via 6X-His tag/Ni-NTA chromatography and then buffer-exchanged into 15 mM pH 8.0 TRIS buffer, 100 mM KCl. Emission spectra of each mutant were collected with a diode array spectrometer, with DPSS laser excitation at 18797 cm^{-1} (532 nm).

Global fitting method

Transients at each wavelength were nonlinear least-squares fitted to a sum of exponential functions convoluted with an instrument response function, which was assumed to be a

Gaussian with a standard deviation of 70 fs determined by the cross correlation between the gate and scattered pump pulse. Amplitudes A(λ) are assumed to be wavelength-dependent with a common set of time constants that applies across the spectra (Equation S1):

$$I(\lambda, t) = \sum_j A(\lambda) e^{-t/\tau_j} \qquad (S1)$$

Initial values for the amplitudes were all set to the amplitude at each wavelength at time zero.

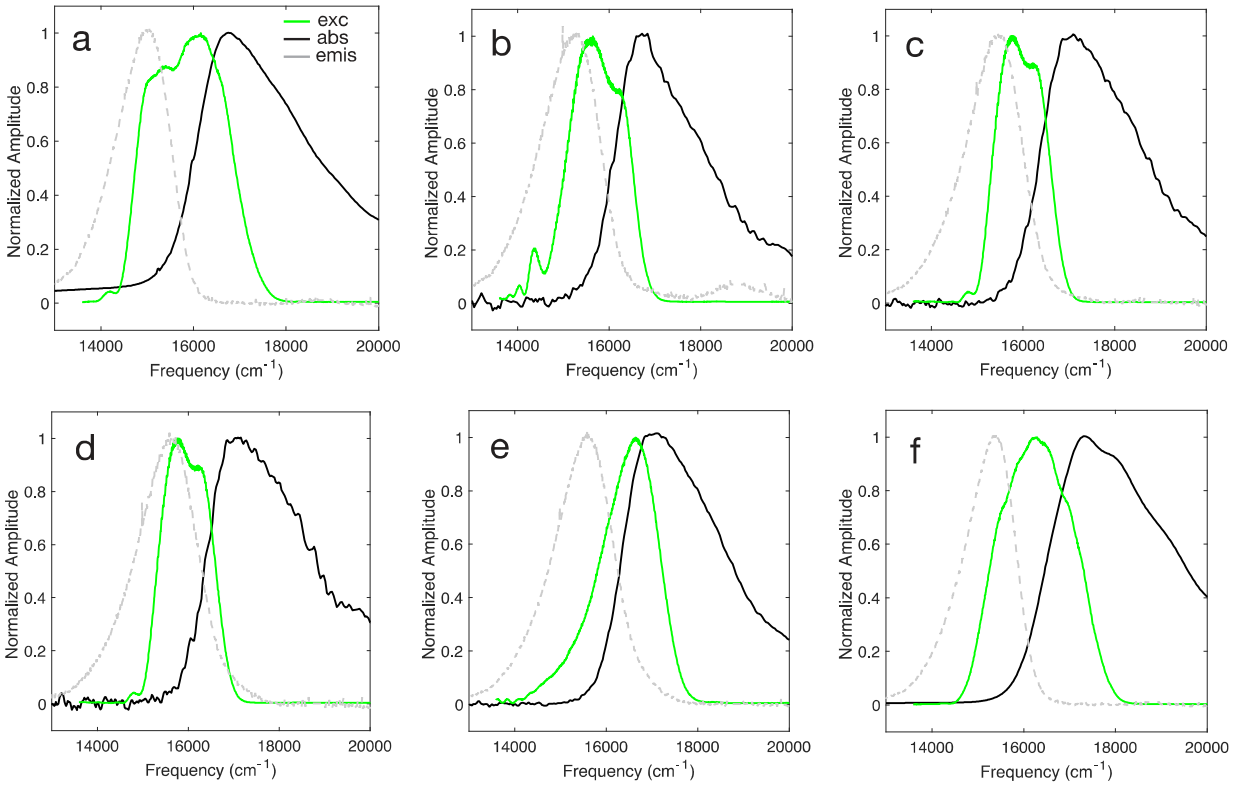

Figure S1. Steady state absorption and emission spectra with SRTG excitation spectra overlaid for (a) TagRFP675, (b) TagRFP675/F62A, (c) TagRFP675/Q106M, (d) TagRFP675/F62A/Q106M (e) TagRFP675/Q41M (f) mKate/M41Q.

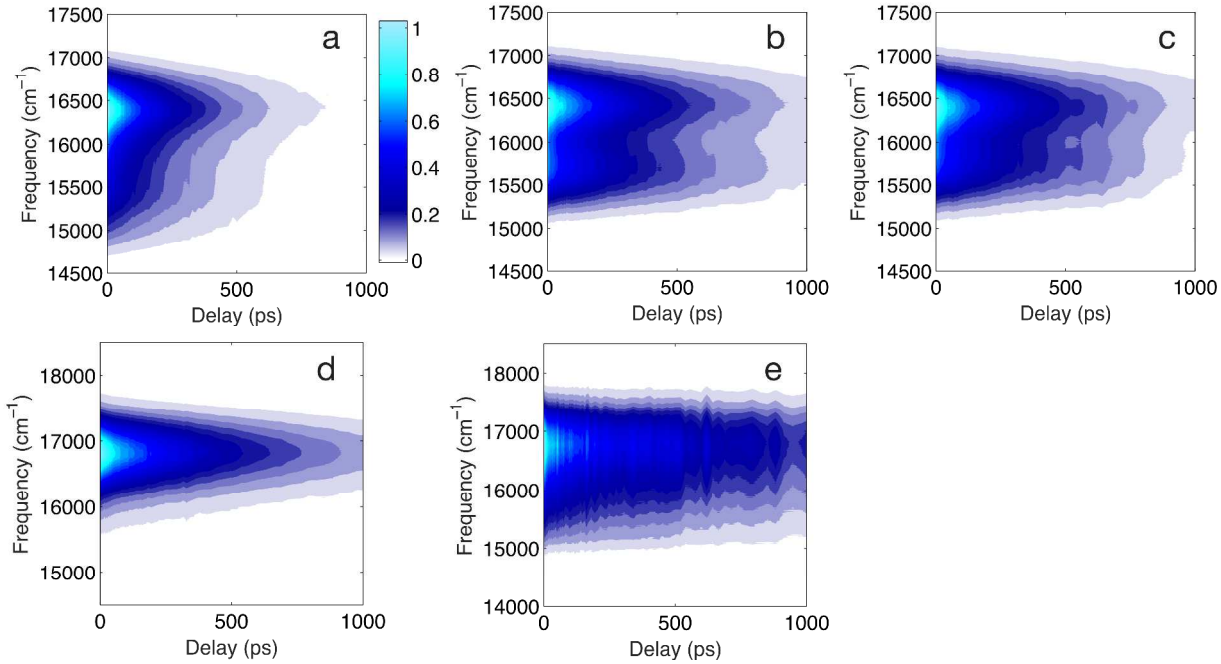

Figure S2. SRTG spectra of (a) TagRFP675/F62A, (b) TagRFP675/Q106M, (c) TagRFP675/F62A/Q106M, (d) TagRFP675/Q41M, (e) mKate

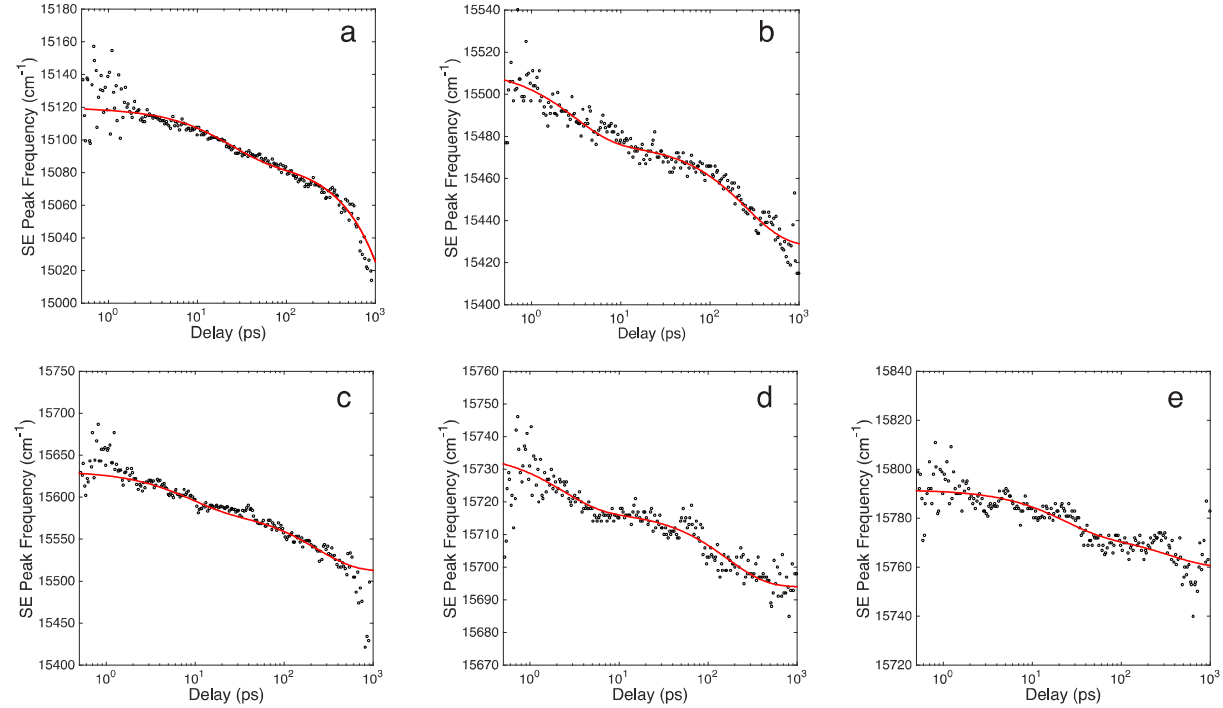

Figure S3. SRTG stimulated emission band peaks *vs.* time determined by fitting each band to a Gaussian function for (a) TagRFP675 and (b) mKate/M41Q, (c) TagRFP675/F62A, (d) TagRFP675/Q106M, (e) TagRFP675/F62A/Q106M. Exponential fits are overlaid in red. Fit parameters given in Table S2.

Table S1. Parameters for the multi-exponential fits to SRTG SE band peak position to the functional form $I(t) = a_1 \exp(^{-t}/_{\tau_1}) + a_2 \exp(^{-t}/_{\tau_2})$

Mutant	a_1 (cm^{-1})	τ_1 (ps)	a_2 (cm^{-1})	τ_2 (ps)
mKate/M41Q	30	5	52	355
TagRFP675	33	17	44	397
TagRFP675/F62A	41	7	68	159
TagRFP675/Q106M	12	4	24	219
TagRFP675/F62A/Q106M	18	24	17	537

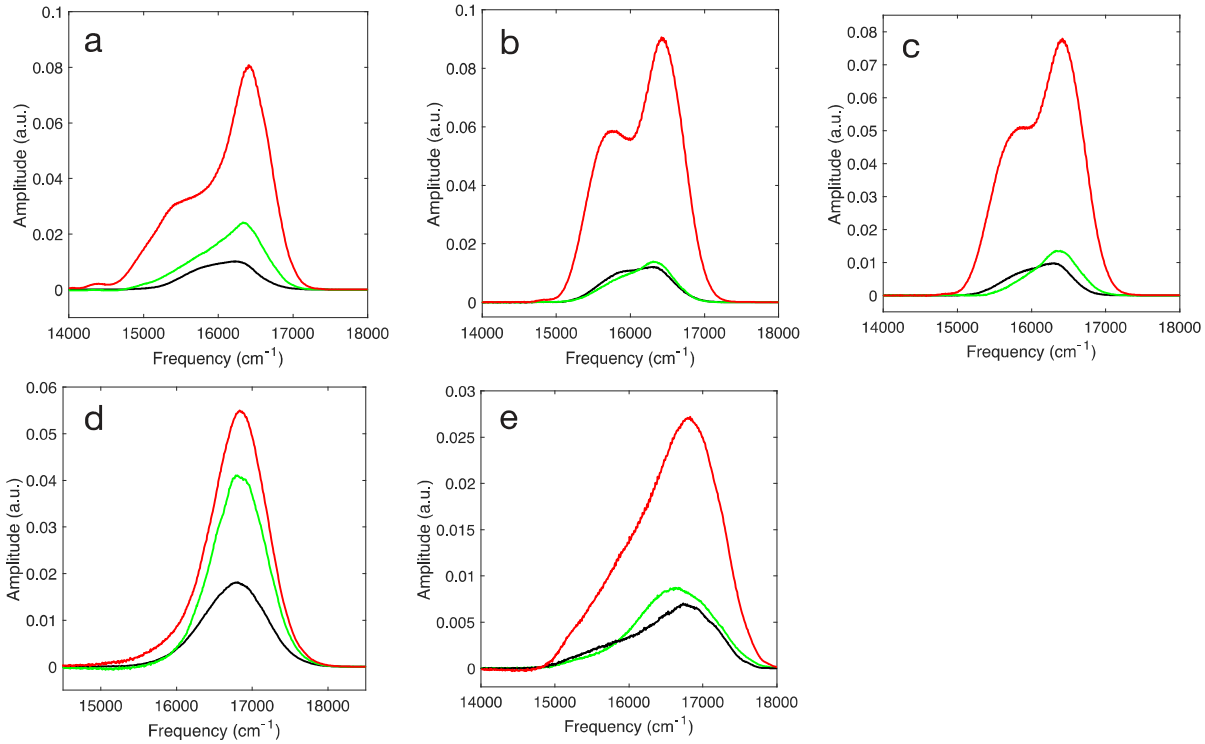

Figure S4. DAS for SRTG of (a) TagRFP675/F62A, (b) TagRFP675/Q106M, (c) TagRFP675/F62A/Q106M, (d) TagRFP675/Q41M, (e) mKate. Time constants for each component are given in Table S2.

Table S2. Time constants for DAS in Figure S4 and Figure 2 tabulated according to color. Red – slowest (τ_1), green - next fastest (τ_2), black -fastest (τ_3).

	τ_1 (ps)	τ_2 (ps)	τ_3 (ps)
TagRFP675	434	134	19
TagRFP675/F62A	585	190	14
TagRFP675/Q106M	794	88	8
TagRFP675/F62A/Q106M	818	112	19
TagRFP675/Q41M	1224	520	88
mKate	1916	142	24
mKate/M41Q	1200	457	9

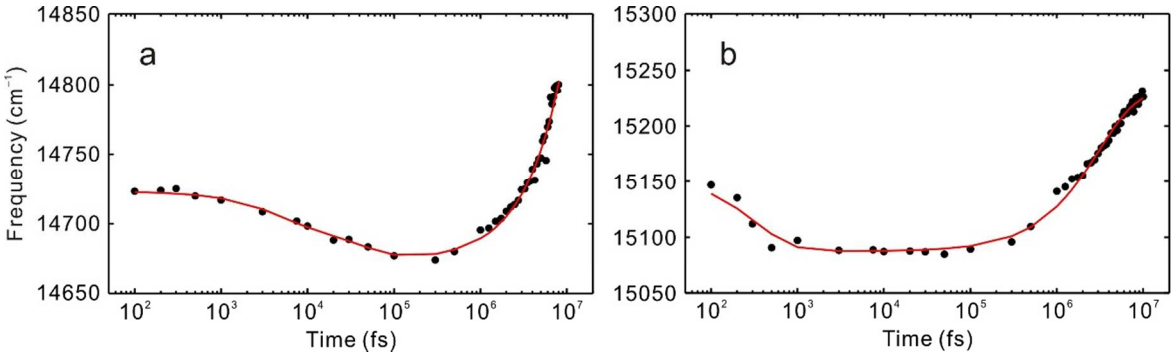

Figure S5. Transient emission peak positions (first moments) extracted from femtosecond and picosecond TRF spectroscopy for (a) TagRFP675 (b) mKate/M41Q.

Table S3. Fit parameters for the time evolution of the first moment of TRF measurements. Fit function is $\nu(t) = a_1 \exp(-t/\tau_1) + a_2 \exp(-t/\tau_2) + \cdots$

Mutant	a_1 (cm^{-1})	τ_1 (ps)	a_2 (cm^{-1})	τ_2 (ps)	a_3 (cm^{-1})	τ_3 (ns)	a_4 (cm^{-1})	τ_4 (ns)
TagRFP675	23	4.5	26	44	1330	16	-3770	23
mKate/M41Q	69	0.33	2	15	-128	5.4		

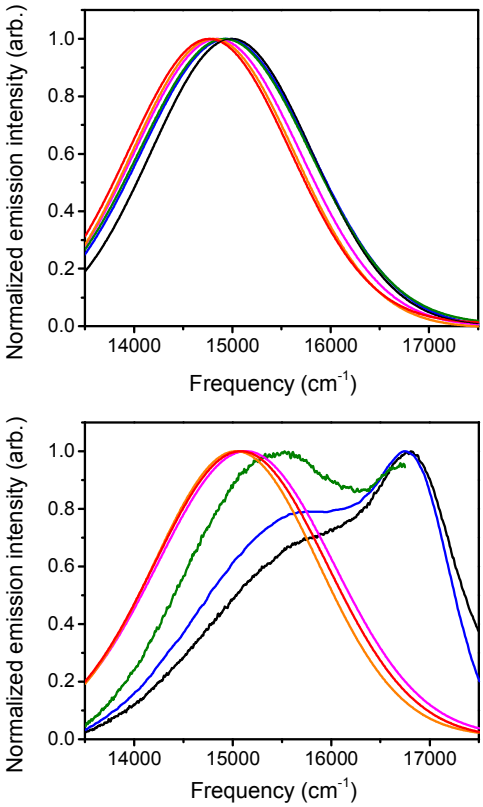

Figure S6. 7. Excitation-dependent emission spectra of (top) TagRFP675 and (bottom) mKate/M41Q. For both plots, the colors correspond to excitation at red-15310 cm^{-1}, orange-15850 cm^{-1}, magenta-16420 cm^{-1}, green- 17040 cm^{-1}, blue- 18050 cm^{-1}, and black- 19190 cm^{-1}.

References

1. Bristow, A. D.; Karaiskaj, D.; Dai, X.; Zhang, T.; Carlsson, C.; Hagen, K. R.; Jimenez, R.; Cundiff, S. T. A Versatile Ultrastable Platform for Optical Multidimensional Fourier-Transform Spectroscopy. *Review of Scientific Instruments* **2009,** *80* (7).
2. Konold, P.; Regmi, C. K.; Chapagain, P. P.; Gerstman, B. S.; Jimenez, R. Hydrogen Bond Flexibility Correlates with Stokes Shift in mPlum Variants. *The Journal of Physical Chemistry B* **2014,** *118* (11), 2940-8.
3. Min, C.-K.; Joo, T. Near-Infrared Cavity-Dumped Femtosecond Optical Parametric Oscillator. *Opt. Lett.* **2005,** *30* (14), 1855-1857.
4. Manoj, P.; Min, C.-K.; Aravindakumar, C. T.; Joo, T. Ultrafast Charge Transfer Dynamics in 2-Aminopurine Modified Double Helical DNA. *Chemical Physics* **2008,** *352* (1-3), 333-338.
5. Phillips, J. C.; Braun, R.; Wang, W.; Gumbart, J.; Tajkhorshid, E.; Villa, E.; Chipot, C.; Skeel, R. D.; Kale, L.; Schulten, K. Scalable Molecular Dynamics with NAMD. *Journal of Computational Chemistry* **2005,** *26* (16), 1781-1802.
6. Brooks, B. R.; Bruccoleri, R. E.; Olafson, B. D.; States, D. J.; Swaminathan, S.; Karplus, M. CHARMM - a Program for Macromolecular Energy, Minimization and Dynamics Calculations. *Journal of Computational Chemistry* **1983,** *4* (2), 187-217.
7. Reuter, N.; Lin, H.; Thiel, W. Green Fluorescent Proteins: Empirical Force Field for the Neutral and Deprotonated Forms of the Chromophore: Molecular Dynamics Simulations of the Wild Type and S65T Mutant. *Journal of Physical Chemistry B* **2002,** *106* (24), 6310-6321.
8. Humphrey, W.; Dalke, A.; Schulten, K. VMD: Visual Molecular Dynamics. *Journal of Molecular Graphics & Modelling* **1996,** *14* (1), 33-38.
9. Essmann, U.; Perera, L.; Berkowitz, M. L.; Darden, T.; Lee, H.; Pedersen, L. G. A Smooth Particle Mesh Ewald Method. *Journal of Chemical Physics* **1995,** *103* (19), 8577-8593.